JOURNAL OF APPLIED ELECTROCHEMISTRY 21 (1991) 377–385

REVIEWS OF APPLIED ELECTROCHEMISTRY 27

# Electrocrystallization: fundamental considerations and application to high current density continuous steel sheet plating*

R. WINAND

*Universite Libre de Bruxelles, CP 165, Department Metallurgy-Electrochemistry, 50 avenue Roosevelt, B-1050 Brussels, Belgium*

Received 17 May 1990; revised 30 July 1990

In this paper, the main factors influencing the morphology of solid metal obtained at the cathode of an electrolytic cell are discussed. Although the presentation is rather fundamental, important practical conclusions are derived. Specific topics linked to electrogalvanizing are stressed.

## 1. Introduction: electrocrystallization

Many factors have an influence on the type of deposit obtained at a cathode: current density, $J$, concentration of the ion containing the metal, $C_{Me^{Z+}}$, agitation, temperature, pH, other cations and anions, complexation, inhibitors, substrate, etc. . . . In order to solve practical problems, a guide is needed for designing the experimental programs if the desired goal is to be reached in a reasonable time.

There is no 'true theory' of electrocrystallization. The field is still largely experimental and is investigated by comparison with *physical crystallization* [1–5]. In the latter case, metal crystals are formed by solidification of the liquid metal or by condensation of the metal vapour, without the presence of foreign atoms and without charge transfer. In the absence of any crystal of the metal, three-dimensional nucleation is first needed. Increasing the supersaturation $S$ (either the difference between the actual temperature of solidification and the melting point of the metal, or the effective vapour pressure against its equilibrium value) increases the rate of three-dimensional nucleation and decreases the diameter of the nuclei.

Essential equations are: first, the work to generate three dimensional nucleus, $A_{c,3}$,

$$A_{c,3} = K\frac{\sigma^3}{S^2} \quad (1)$$

where $\sigma$ is the interfacial tension solid/fluid, $S$ the supersaturation, and $K$ a constant; second, the three dimensional nucleation frequency, $N_{c,3}$,

$$N_{c,3} = C\exp\left(-\frac{A_{c,3}}{kT}\right) \quad (2)$$

where $k$ is the Boltzmann's factor, $T$ the absolute temperature, and $C$ a constant.

An important experiment by Volmer and Estermann [1] showed surface diffusion of adatoms to occur, resulting in the concept of two dimensional nucleation (generating a new plane on a crystal surface) and one-dimensional nucleation (generating a new row on a crystal surface).

Until it was realized that crystal growth can occur by means of spiral growth originating at a screw dislocation [6], ideas of Kossel and Stranski [1] were largely accepted: growth occurs in repeatable monoatomic layers following two dimensional nucleation. Many experimental facts show the importance of this growth process in the electrodeposition of metals. Owing to the fact that lattice forces in metals have very short ranges of influence, the probability of incorporation of an atom at the surface of a crystal is the highest where the largest number of neighbours is available. This is shown in Fig. 1, where the most probable incorporation site is 1/2, the so-called kink site, which is at the same time a repeatable step. When the row is completed, the next best position is 6, creating a new one dimensional nucleus along the developing plane. When this one is completed, the next best position is 7, and a new two-dimensional nucleus is formed.

According to this model, the growth of a single crystal occurs through competition between vertical growth (depending on two-dimensional nucleation rate) and horizontal growth (depending on the rate of the repeatable step).

On this basis, the external shape of a perfect crystal grown almost at equilibrium can be found: faces where the energy of incorporation of an atom in position 7 is the lowest are maintained, because they have time to develop laterally. For f.c.c. metals (Cu, Ni, Co$\beta$, Au, Ag), (1 1 1) planes give tetragonal pyramids; other possible planes are (1 0 0) resulting

* Based on a Keynote Lecture given at The International Conference on Zinc and Zinc Alloy Coated Steel Sheet (GALVATECH, Tokyo), 1989, organized by the Iron & Steel Institute of Japan.

0021-891X/91 $03.00 + .12 

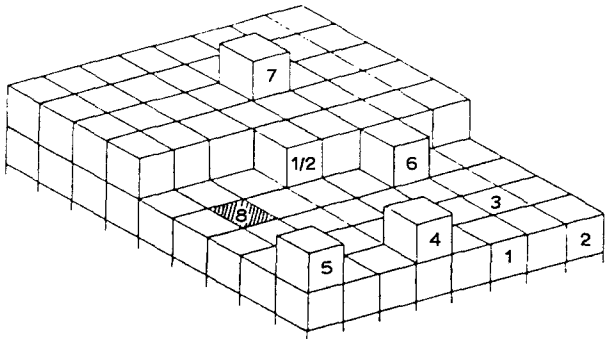


Fig. 1. Schematic drawing of a single cubic lattice showing different possible sites of incorporation of an atom in the lattice [5].

in cubes, and (1 1 0) corresponding to rhombododecahedrons. For h.c.p. metals, (Zn, Cd, Coα), limiting planes should be (0 0 1) resulting in hexagonal prisms.

At increasing supersaturation, more than one step can grow at the same time so that other limiting planes appear, the external shape becomes round, dendrites or whiskers appear and finally new three-dimensional nuclei appear.

In electrocrystallization, the problem is more complicated than in physical crystallization due to charge transfer to a more or less solvated ion, to the very high electric field at the electrode-solution interface ($10^7\,V\,cm^{-1}$), and to the presence of adsorbed molecules and ions at the surface of the electrode.

Accordingly, a pragmatic approach is used: as for physical crystallization, a correlation is sought between the observed crystalline shapes of the deposits and a measurable physical parameter characteristic of the supersaturation, i.e. the cathodic overpotential.

Overpotential is however a complex parameter. According to Vetter [7], it can be separated into four additive terms: charge transfer overpotential, $\eta_t$, diffusion overpotential, $\eta_d$, reaction overpotential, $\eta_r$, and crystallization overpotential, $\eta_{cr}$.

At first sight, only the crystallization overpotential should be taken into consideration. However, it is difficult to measure and is usually obtained by subtracting the other types of overpotentials from the total overpotential, so that accuracy is very low. Further, a detailed analysis shows that the other types of overpotential must also be taken into account because they influence the total distribution of current density and also the equilibrium concentration of adatoms.

On this basis, Winand suggested [2–5] making use of two further important parameters: the ratio $J/J_{dl}$ between the apparent cathodic current density and the diffusion limiting current density, and the inhibition intensity.

Although the approach was initially mainly intuitive, reasons for the choice of those two parameters can be explained as follows [5]. The ratio $J/J_{dl}$ is directly characteristic of mass transfer to the electrode. The two main equations are:

$$\eta_d = \frac{RT}{nF} \ln (1 - J/J_{dl}) \qquad (3)$$

where $R$ is the perfect gas constant, $T$ the absolute temperature, $n$ the number of electrons involved in the cathode reduction, and $F$ the Faraday; and

$$J_{dl} = \frac{n}{v_j} F \frac{D_j}{\delta} \bar{c}_j \qquad (4)$$

where $v_j$ is the stoichiometric coefficient of the species $J$ to reduce at cathode in the electrochemical reaction, $D_j$ the diffusion coefficient of $j$, $\delta$ the thickness of the diffusion layer, and $\bar{c}_j$ bulk concentration of $j$.

For charge transfer, the overpotential may be written:

if $\eta_t$ is low

$$\eta_t = \frac{RT}{zF} \frac{J}{J_0} \qquad (5)$$

if $\eta_t$ is high

$$\eta_t = \frac{RT}{(1 - \alpha)zF} \ln J_0 - \frac{RT}{(1 - \alpha)zF} \ln J \qquad (6)$$

and

$$J_0 = k_- c_0$$

where $z$ is the charge of $j$, $\alpha$ the energy transfer coefficient, $J_0$ the exchange current density, $k_-$ the kinetic constant of cathode reduction, and $c_0$ the concentration of $j$ at surface of electrode.

In fact,

$$c_0 = \bar{c}_j(1 - J/J_d) = \bar{c}_j - \frac{v_j}{nFD_j} J\delta \qquad (7)$$

and finally $c_0$, $J_0$ and thus $\eta_t$, are functions of $J$, $\bar{c}_j$, and $\delta$.

Accordingly, at any spot, on a diagram having $J/J_{dl}$ and inhibition intensity as coordinates, it should be possible to assign a value for $\eta_d$ and $\eta_t$, provided the hydrodynamics of the electrolyte flow is known. The same type of analysis, more complicated however, would show that $\eta_r$ and $\eta_{cr}$ could also be calculated at any spot on the diagram, provided $J$, $\bar{c}_j$, $\delta$ are known.

If mass transfer is readily understandable, inhibition deserves more explanation. According to Fischer [1, 8], inhibition is due to the presence at the surface of the electrode, in the double layer or in the diffusion layer, of substances (molecules, atoms or ions) different from the cation to be discharged or the corresponding adatom. These substances hinder the cathodic process and are called inhibitors. They usually do not cover the cathode surface completely and favour active sites. They are physically or chemically adsorbed. They have a dramatic influence on the metallographic structure and the crystallographic texture of deposits, and they also influence overpotential.

Sensitivity of metals to inhibition depends on the 'affinity' of surface atoms of the metal for the inhibitor and on the surface diffusion coefficient of adatoms. Accordingly, it hangs on the nature of the metal (normal metal: low melting point, low charge transfer overpotential with high exchange current density and high surface diffusion coefficient of adatoms show low

inhibition sensitivity; inert metals: with reverse properties and show high inhibition sensitivity; in between; intermediate metals).

Different types of inhibitors are: inorganic cations; inorganic anions; organics in solution; organics in colloidal suspension. Another type of inhibition may arise from the cathode reduction process itself: if hydrogen evolution occurs, local pH may raise to a value at which hydroxide precipitation occurs, resulting in so called secondary inhibition; also, an adsorbed layer of partially reduced metal hydroxide may be involved in the cathode reduction mechanism, playing the same role.

Finally, inhibition intensity is clearly a complex parameter, not yet fully understood [9]. It should also be pointed out that organic inhibitors undergo complex chemical, electrochemical and mechanical degradation in the electrolytic tank, the pumping system, the storage tanks and the eventual filters, so that most laboratory scale experiments, performed with an initial addition of organics at the beginning of the electrolysis, are not relevant.

Despite these difficulties, in this paper inhibition intensity will be considered as linked in a biunivoqual relationship to the concentration of a given species in solution or adsorbed at the surface of the metal: the inhibitor.

Experimental work largely shows that, for three dimensional nucleation, the same observations are made in electrocrystallization and in physical crystallization: increasing $J/J_{dl}$ and/or inhibition intensity results in an increase of the rate of nucleation and in a decrease in grain size in the deposit. Concerning single crystal growth, although a few experiments showed evidence of growth on screw dislocations without mono- and two-dimensional nucleation, it was shown that screw dislocations become inactive at low inhibition intensity [10]. On the other hand, many authors observed moving layers at the surface of a metal undergoing cathodic deposition. Budevski [11] was even able to initiate such growth layers by potential pulses. It may thus be concluded that for deposits obtained under industrial conditions two-dimensional nucleation plays the important role in crystal growth. Of course, electrodeposited crystals contain dislocations, but they do not seem to be active for crystal growth. Also, the growth layers are thicker than monoatomic due to bunching effects occurring because of adsorbed impurities. The external shape of the crystal depends on the competition between two-dimensional nucleation (vertical growth) and the lateral growth of the layer formed by bunching of the initial monoatomic layers.

Concerning polycrystalline electrodeposits, after eventual three dimensional nucleation (if no epitaxy occurs on the substrate crystals), many crystals are developing at the same time, as in every industrial electrodeposit. Lateral growth may be stopped either due to a lack of local current density or because of the presence of the next crystal. On the basis of competition between vertical and lateral growth, and also taking into account eventual three-dimensional nucleation if sufficient energy is available, Winand [2–5] derived a diagram (Fig. 2) showing the fields of predominance of the four main types of deposits according to Fischer [1]:

field oriented isolated crystals type (FI)
basis oriented reproduction type (BR)
field oriented texture type (FT)
unoriented dispersion type (UD).

Other types can be observed:

twinning intermediate type (Z), occurring generally between FI and FT

nodular type (N), occurring when fine electronic conducting or semiconducting solids in suspension in the electrolyte are trapped at the surface of the deposit, or appear due to degradation of organic additives

rhythmic lamellar type (RL), occurring when some unstable reaction mechanism occurs at the cathode.

The validity of this diagram was checked in the author's laboratory initially without organic additives. Comparing structures obtained for silver in nitrate solutions [12], for copper in sulphate solutions [13, 14], for copper in chloride solutions [15, 16] and for cobalt in chloride solutions [17], it appears that when no organic inhibitor is present, inhibition intensity may be characterized by the value of the exchange current density $J_0$: the lower $J_0$, the higher the inhibition intensity. It was also observed that the sensitivity to organic inhibitors of these electrolytes is low when $J_0$ for the electrolyte without organic additive is high [18–22].

On the other hand, transition between FT and UD types of deposits was observed for copper deposition from pure sulphate solution at a constant value of $J/J_{dl}$, for various current densities and speeds of electrolyte flowing in a channel cell [23].

## 2. High current density plating for coil coating

Owing to the fact that organic additives are difficult to control in industrial practice (active species unknown; the initial molecule undergoes degradation processes leading to new molecules eventually active in a different way than the original one; analytical problems due to low additive concentrations in concentrated salt solutions; erratic monitoring), most high current density coil coating processes were developed without organic additives. In this case, the main controlling factor is the ratio $J/J_{dl}$.

Accordingly, special care must be taken in the electrolytic cell to keep hydrodynamic conditions and current density constant over the whole cathode surface. This is not easy to achieve, and it is beyond the scope of this paper to discuss advantages and disadvantages of industrial and prototype cells now available or under development. It seems, however,

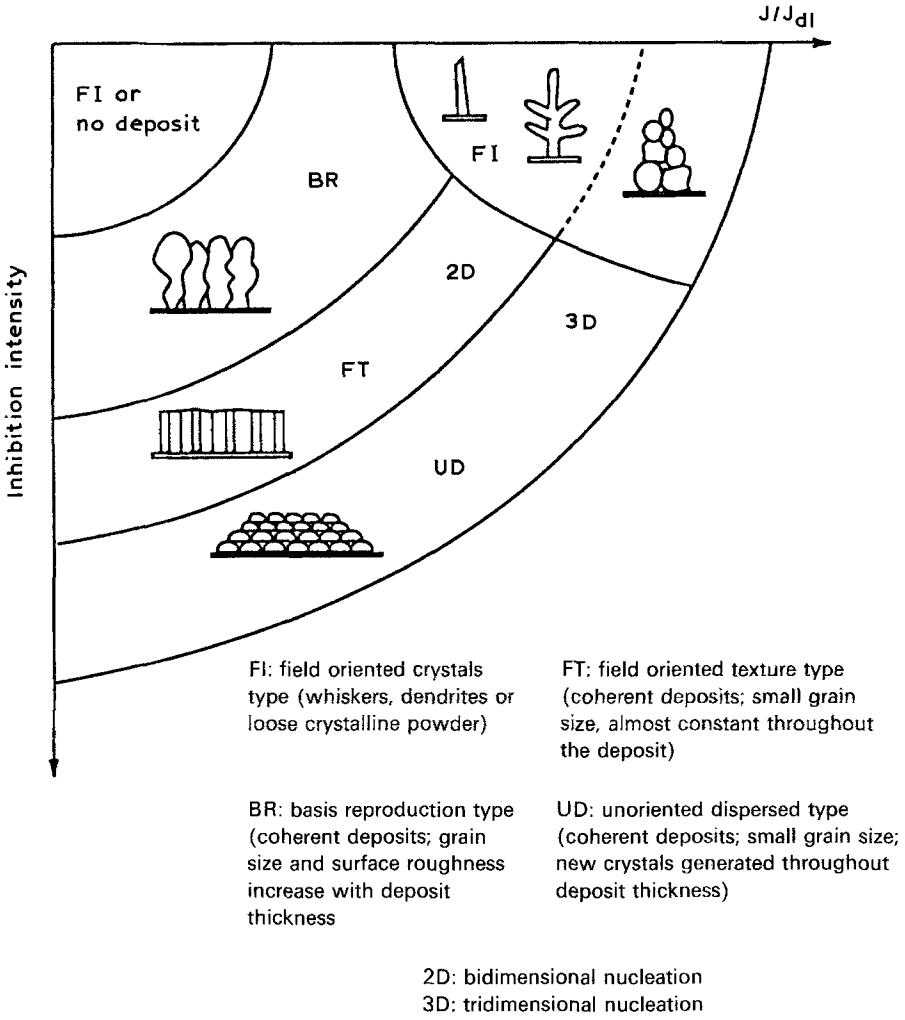


Fig. 2. Fields of stability of the main deposit structures.

that designs based on flow through channel cells (linear or curved) and on current feed on the whole cathode area have the best chances of success.

In the author's laboratory, channel cells were used to deposit copper [23, 24, 25], zinc [26, 27], manganese [28, 29], and zinc alloys [30, 31, 32]. The first very striking observation is the possibility of plating with direct current up to very high current densities, in the range of several hundred A dm$^{-2}$. This is due to the high values of $J_{dl}$ that can be achieved by flowing the electrolyte parallel to the electrodes: values as high as 1200 A dm$^{-2}$ could be measured making use of the tracer technique in a zinc sulphate electrolyte [33]. However, besides the electrolyte flow, hydrogen evolution at the cathode was also shown to have an important influence on $J_{dl}$. For instance, it was shown in a laboratory scale channel cell [31, 32] that, when plating zinc–iron alloys from sulphate solutions at an electrolyte flow rate of 2 m s$^{-1}$, mass transfer coefficient for $Zn^{2+}$ could be written as [33]:

$$k_{Zn^{2+}} = 0.67 \times 10^{-2} + 0.16 \times 10^{-3} J_{H_2}^{1/2}$$

where $k_{Zn^{2+}}$ is in cm s$^{-1}$ and $J_{H_2}$ in A cm$^{-2}$.

In this equation illustrated in Fig. 3, the first term is due to forced convection due to the flow of the electrolyte and is proportional to that velocity of exponent 0.8 (see Fig. 4), while the second term is the contribution of hydrogen evolution. It appears that if current efficiency is low at high current density, $k_{Zn^{2+}}$ could be increased easily by a factor of two due to hydrogen evolution. This should be kept in mind when studying new processes or new alloys. For pure zinc, current efficiencies are fairly high over a wide range of current densities (Fig. 5), so that this effect is rather

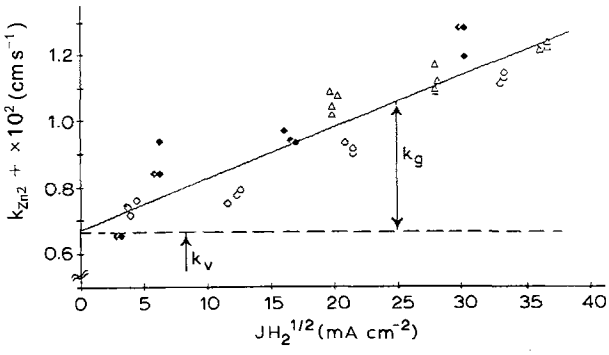


Fig. 3. Relation between the mass transfer coefficient for zinc and the square root of the hydrogen partial current density. Zn–Fe sulphate electrolytes: 0.2 M $H_2SO_4$; 50° C; Electrolyte velocity: 2 m s$^{-1}$ [33]. (◆) Fe: 0.75 M, Zn: 0.75 M; (◇) Fe: 1 M, Zn: 0.5 M; (△) Fe: 1 M, Zn: 0.1 M.

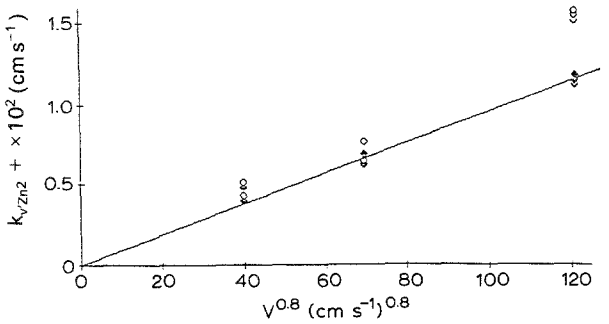


Fig. 4. Relation between the mass transfer coefficient for zinc due to macroconvection and the electrolyte flow rate. Zn–Fe sulphate electrolytes: 0.2 M $H_2SO_4$; 50° C. The Chilton Colburn equation is verified with exponent 0.8, characteristic of turbulent flow [33]. (◆) Fe: 1 M, Zn: 0.1 M; (◇) Fe: 1 M, Zn: 0.5 M.

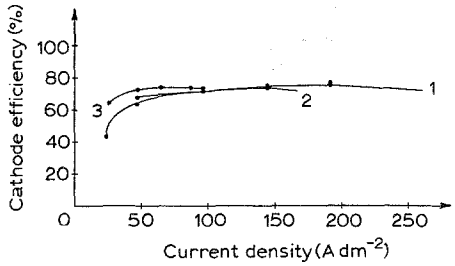


Fig. 6. Cathode current efficiency as a function of current density for zinc–nickel alloy plating for: 50 g l$^{-1}$ $Zn^{2+}$; 30 g l$^{-1}$ $Ni^{2+}$; 35 g l$^{-1}$ $H_2SO_4$, channel cells at 50° C and electrolyte velocity at 1–3 m s$^{-1}$. Deposit thickness: 5–10 μm [30].

weak. This is not the case for alloys: zinc–nickel alloys are obtained with current efficiencies between 70 and 80% (Fig. 6) and the situation is even worse for zinc–iron (Fig. 7). Of course, in the latter case, control of electrolysis parameters must be more precise than in the two other ones because there is no range of current density where current efficiency may be considered as constant: changes in alloy composition and in deposit structure could occur.

Metallographic cross sections for thin deposits are difficult to prepare and etch properly, especially for pure zinc. However, Rodriguez [31, 32] succeeded in studying completely the system Fe–Zn by this method. Various observed structures are shown in Figs 8 and 9. It should be emphasized that, although difficult, this kind of study is very useful and shows interesting features, not directly available by surface examination. In the case of the zinc–iron system, on the zinc rich side, an initially named UD structure was found later to be an overetched BR structure, so that the final diagram summarizing all structures is given in Fig. 10. It shows that pure zinc deposits change from BR to FT structures when current density increases, and that a rather large field of FT structures is observed for deposits containing less than 30% iron. Above this limit, nodular or rhythmic lamellar structures are observed. At the top of the diagram, pure iron deposits are often of the FT type.

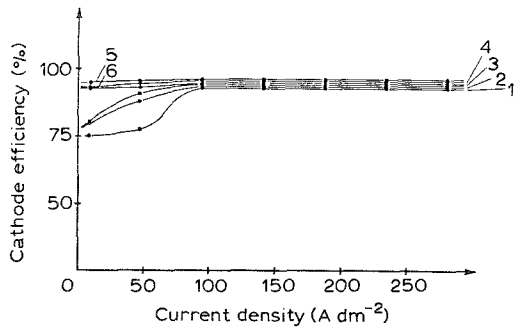


Fig. 5. Cathode current efficiency as a function of current density for zinc plating for 80 g l$^{-1}$ $Zn^{2+}$; 135 g l$^{-1}$ $H_2SO_4$, channel cell at 50° C and electrolyte speed at 4 m s$^{-1}$. Theoretical deposit thickness: (1) 5 μm; (2) 10 μm; (3) 25 μm; (4) 50 μm; (5) 100 μm; (6) 200 μm [26].

Surface microscope examination is also useful. However, grain size may not be determined on this basis and, as already said, hidden structure features are not shown as exemplified by Fig. 11, where the rhythmic lamellar or nodular structures of deposits at 36 and 54% Fe are not clearly seen.

Surface appearance, although somewhat subjective, is very important in practice and frequently determines the useful range of electrolysis parameters. Figure 12 gives such a diagram for zinc in pure sulphate solutions, showing again that very high current densities may be used. This diagram may be related to surface microscope examination, surface roughness and grain size. Generally, when $J/J_{dl}$ increases, surface roughness increases at constant deposit thickness. The situation is not so clear for grain size, although a general trend towards a decrease in grain size when $J/J_{dl}$ increases is commonly accepted [35].

Of course, the deposit thickness is a very important factor: when no organic additive is present, surface

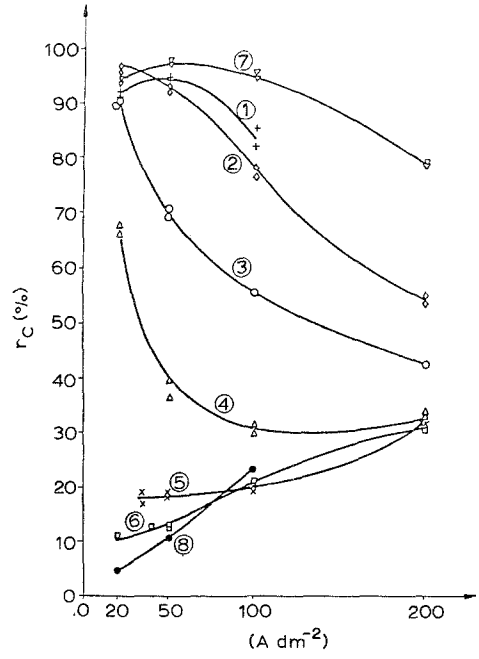


Fig. 7. Cathode current efficiency as a function of current density for zinc–iron alloy plating. Channel cell deposit thickness 5–10 μm [32]; electrolyte velocity: 2 m s$^{-1}$ for 0.2 M $H_2SO_4$. T: 50° C 1. (+) Fe: 1 M, Zn: 1 M; 2. (◇) Fe: 0.75 M, Zn: 0.75 M; 3. (○) Fe: 1 M, Zn: 0.5 M; 4. (△) Fe: 1 M, Zn: 0.2 M; 5. (×) Fe: 1 M, Zn: 0.1 M; 6. (□) Fe: 1 M, Zn: 0.05 M; 7. (▽) Fe: 0.375 M, Zn: 1.125 M; 8. (●) Fe: 1.5 M, Zn: –.

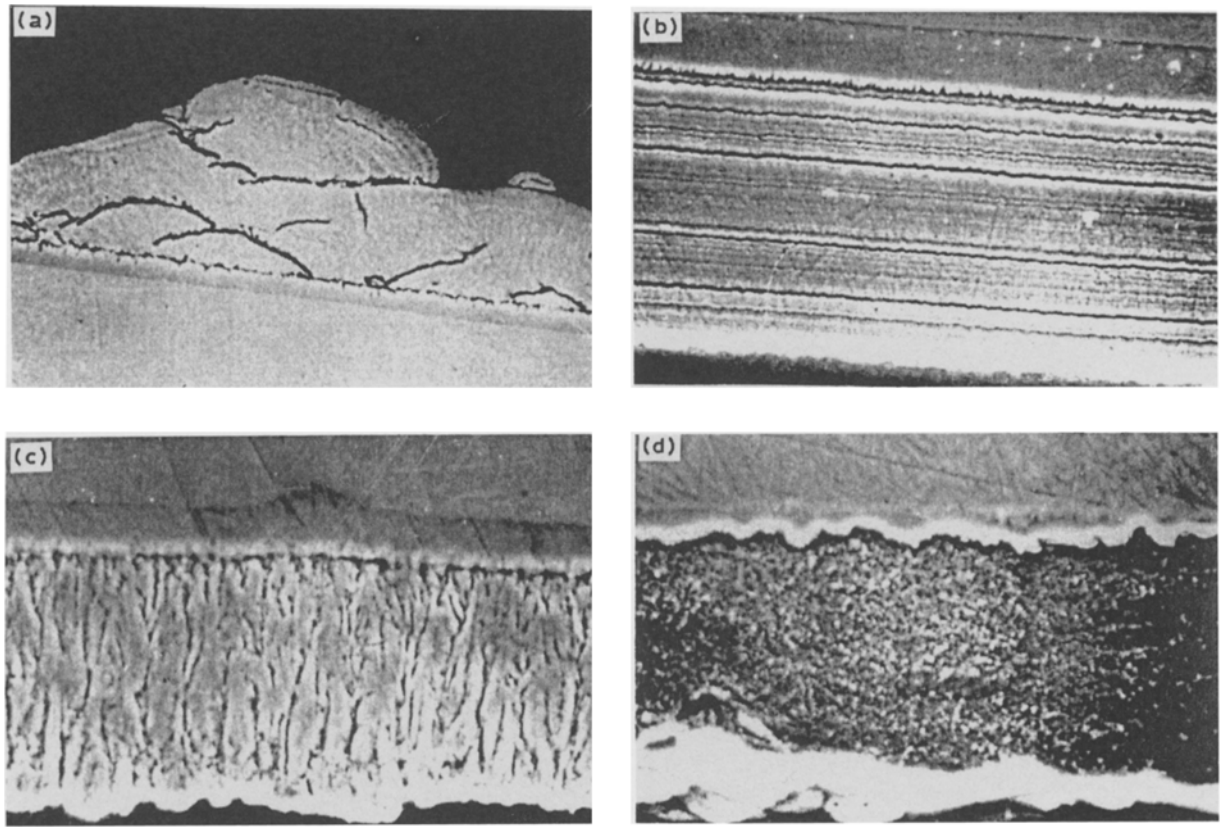


Fig. 8. Various metallographic structures observed in the system Fe–Zn: N, RL, FT and pseudo UD (later shown as BR) structures are observed [32]. (a) Nodular (N), (b) rythmic lamellar (RL), (c) field orientated (FT) and (d) unorientated dispersed (UD).

roughness increases with deposit thickness, ending in nodular or dendritic structures. Figure 13 shows the degradation of the surface of a pure zinc deposit when its thickness reaches 200 $\mu$m. Although the metallographic cross section shows a BR compact structure, open porosity is evident and multiple two-dimensional nucleation leads progressively to FI structures.

Crystallographic texture orientation is also of interest. For pure zinc, the following sequence was observed [27] when current density increases: $(1\,1\,\bar{2}\,2)$–$(1\,0\,\bar{1}\,1)$–$(0\,0\,0\,2)$–$(1\,0\,\bar{1}\,0)$ with a wide range of stability of $(0\,0\,0\,2)$. For zinc alloys, as usually observed in electrodeposition, phases determined by X-ray investigation are different from thermal equilibrium. Figure 14 gives as example the case of zinc–iron alloys. This is of course of importance for corrosion properties, and also for mechanical properties necessary for forming, especially in deep drawing [36, 37].

Alloy composition changes of course with electrolysis conditions. Figures 15 and 16 show that both Zn–Ni and Zn–Fe alloys pertain to the anomalous codeposition, iron being codeposited only when enough iron is present in solution [36].

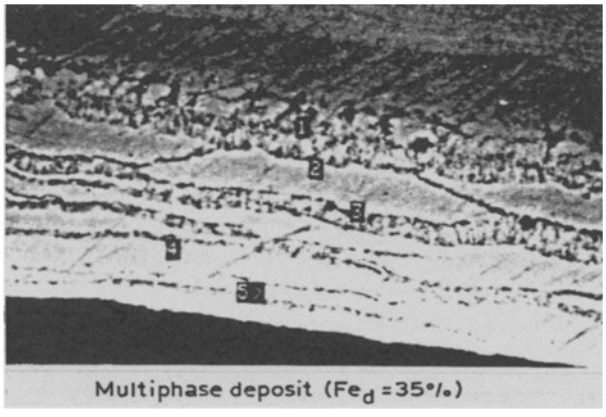


Fig. 9. Detail of a metallographic structure obtained for a multiphase Fe–Zn deposit (35% Fe) [32].

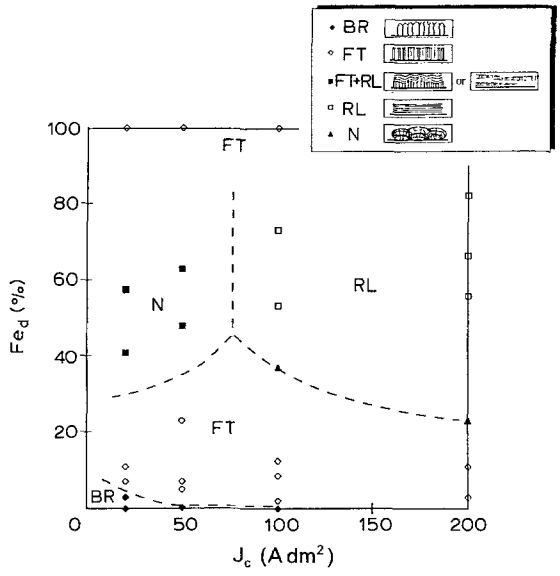


Fig. 10. Cross section metallographic structures of alloy deposits as a function of current density and composition. Channel cell: 0.2 M $H_2SO_4$ with $Fe^{2+}$ and $Zn^{2+}$ as sulphates at 50° C. Electrolyte speed: 2 m s$^{-1}$ [34].

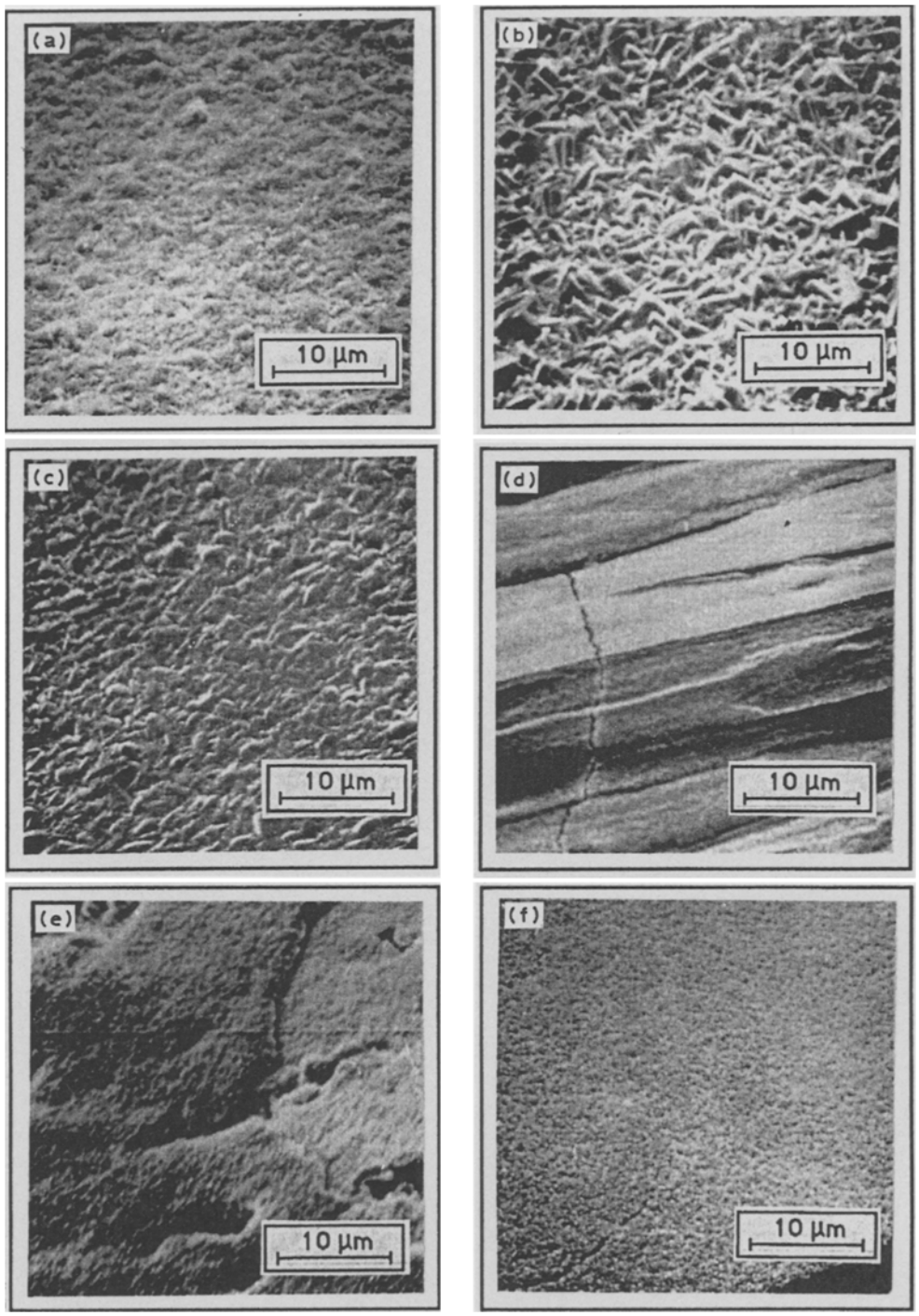


Fig. 11. Surface microscope examination of various Fe–Zn deposits. Channel cell: 0.2 M $H_2SO_4$ with $Fe^{2+}$ and $Zn^{2+}$ as sulphates at 50° C. Electrolyte velocity: 2 m s$^{-1}$ current density 100 A dm$^{-2}$ [32]. (a) $Fe_d$ = 1%, (b) $Fe_d$ = 10%, (c) $Fe_d$ = 13%, (d) $Fe_d$ = 36%, (e) $Fe_d$ = 54% and (f) $Fe_d$ = 100%.

## 3. Research needs

Since most high current density coil coating plants do not use organic additives, every effort should be made to keep the ratio $J/J_{dl}$ as constant as possible throughout the electrolytic cells. When cell design does not allow this to be achieved easily, hydrodynamics should be carefully characterized so that, by changing anode positions, satisfactory stable $J/J_{dl}$ ratios can be maintained. This is especially true for zinc alloys, where not only surface appearance, but also alloy composition and metallographic structure are influenced by this factor. Tracer methods seem particularly promising to

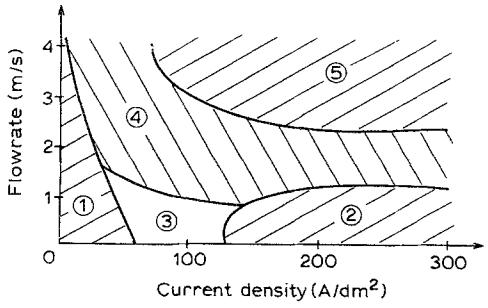


Fig. 12. Surface appearance of zinc deposits as a function of flowrate and current density: (1) non uniform, including bare areas not covered by the deposit; (2) black with poor quality; (3) uniform, but very porous at the surface; (4) homogeneous, but rather rough; (5) macroscopically uniform, smooth, and bright or glazed [27].

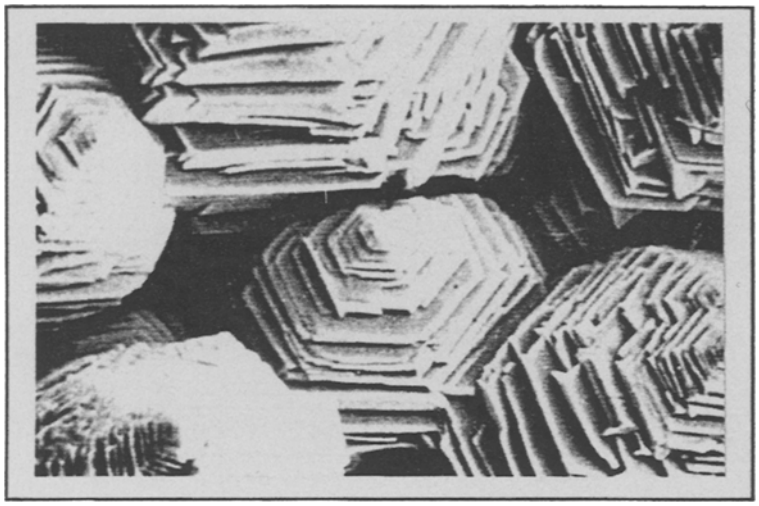

Fig. 13. Surface of a 200 $\mu$m thick compact zinc deposit obtained at a flowrate of 4 m s$^{-1}$ and 150 A dm$^{-2}$. Channel cell at 50° C with 80 g l$^{-1}$ $Zn^{2+}$ as sulphate and 130 g l$^{-1}$ $H_2SO_4$. Magnification: 900 × [27].

determine local $J_{dl}$ values. A good review of the subject may be found in [33].

Another way to improve deposit quality when $J/J_{dl}$ control is not easily achieved is to make use of organic additives. This may result in enlarging the field of $J/J_{dl}$ values giving constant deposit properties. However, this means a considerable research effort to understand the organic additive chemistry and electrochemistry, in order to be able to maintain constant the inhibition intensity. Monitoring problems should also be solved. An introduction to the subject may be found in [38].

Adhesion to the substrate seems to be satisfactory in most cases. However, if adhesion bonding is to replace welding in the future, this specific point should be investigated in detail, not only in connection with substrate cleanliness and roughness, but also by finding ways of promoting surface activation in order to obtain some nanoalloying effect.

Nucleation should also be investigated in greater detail, not only from the theoretical standpoint, but also in order to derive what influence this phenomenon could have on deposit properties such as grain size, texture, metallographic structure and mechanical properties. In fact, thin deposits in the range of a few micrometers do not grow according to their stationary structure type, and the diagram shown in Fig. 2 should be redrawn for the initial stages of deposition. It is beyond the scope of this paper to discuss nucleation in electrocrystallization. However, fundamental and applied research is active in the field, but usually at rather low current densities. Some interesting papers are to be found [39 to 41].

Ultrathin deposits like Cr–CrOx (100 nm) are certainly even more influenced by nucleation. In this case, other factors like interfacial tension and possible underpotential deposition should also be studied.

Finally, future alloys will almost certainly include a class of microalloys. Zn–Co alloys with cobalt content lower than 1% are already in use [36, 37]. Others may be developed, aimed at specific properties such as adhesion, surface appearance, deep drawing lubrication, etc. This stresses the need for a good definition of functional properties, so that the electrolytical process can be optimized to achieve at best the final materials requirements.

## 4. Conclusions

High current density electrocrystallization is feasible up to very high direct current densities (300 to 500 A dm$^{-2}$). Most coil coating processes work with-

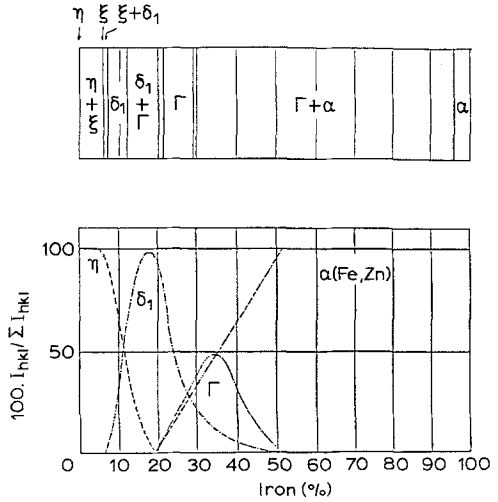


Fig. 14. Comparison of electrodeposited phases with those from thermal equilibrium for iron–zinc alloys [32].

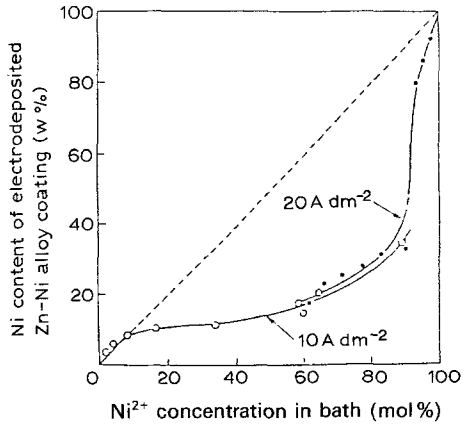


Fig. 15. Electrodeposition of Zn–Ni alloy from sulphate bath showing anomalous codeposition [36]. $Zn^{2+}$ + $Ni^{2+}$ 1.5 M; pH 2.0; $T$ = 50° C.

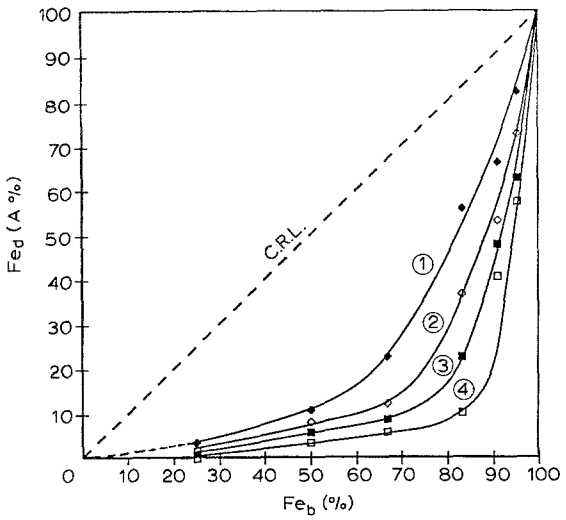


Fig. 16. Atomic percentage of iron in Fe–Zn alloy from sulphate electrolyte against Fe/Fe + Zn in electrolyte at 50° C and electrolyte velocity $2\,m\,s^{-1}$ with $H_2SO_4$: 0.2 M at: (1) $200\,A\,dm^{-2}$, (2) $100\,A\,dm^{-2}$, (3) $50\,A\,dm^{-2}$, and (4) with $20\,A\,dm^{-2}$.

out organic additive, so that the controlling parameter is the ratio $J/J_{dl}$ of the current density to the diffusion limiting current density. Design of electrolytic cells should accordingly allow achievement of uniform current density and constant hydrodynamic conditions. Research needs are in the field of hydrodynamic characterization of electrolytic cells, of eventual organic additive chemistry and electrochemistry, of adhesion of deposits to substrate, of nucleation, of ultrathin and of microalloyed deposits.

## References


[1] H. Fischer, 'Elektrolytische Abscheidung und Elektrokristallisation von Metallen', Springer Verlag, Berlin (1954).

[2] R. Winand, 'Contribution à l'étude de l'électrocristallisation en sels fondus et des phénomènes connexes – Application au cas particulier du zirconium', Ph.D. Thesis, Université Libre de Bruxelles (1960).

[3] *Idem, Mém. Scient. Revue Mét.* **58** (1961) 25–35.

[4] *Idem, Trans./Sect. C, IMM* **84** (1975) 67–75.

[5] *Idem*, in 'Application of polarization measurements in the control of metal deposition', Process Metallurgy, (edited by I. H. Warren), Elsevier, Amsterdam (1984) pp. 47–69.

[6] W. K. Burton, K. Cabrera and F. C. Frank, *Nature* **163** (1949) 398–9.

[7] K. J. Vetter, 'Electrochemical kinetics', Academic Press, New York (1967).

[8] H. Fischer, *Electrochim. Acta* **2** (1960) 50–96.

[9] R. Winand, G. Troch, M. Degrez and Ph. Harlet, in I. H. Warren (ed.) *op. cit.* [5], pp. 133–45.

[10] H. Seiter, H. Fischer and H. Albert, *Naturwissensch.* **45** (1958) 127.

[11] E. Budevski, *J. Crysta. Growth* **13/14** (1972) 93–6.

[12] J. Cl. Evenepoel and R. Winand, *Revue ATB Mét.* **10** (1970) 133–46.

[13] R. Winand and A. Fontana, *Trans. Sect C. Inst. Mining and Met.* **84** (1975) 67–76.

[14] K. B. Tshula, 'Contribution à l'étude de l'électroraffinage du cuivre', Ph.D. Thesis, Université Libre de Bruxelles (1983).

[15] L. Albert and R. Winand, 111th AIME annual meeting, Dallas (February 1982), TMS paper selection no. A82-26.

[16] P. A. Andrianne, J. P. Dubois and R. Winand, *Met. Trans. AIME,* **8B** (1977) 315–21.

[17] J. Scoyer and R. Winand, *Surface Technology* **5** (1977) 169–204.

[18] J. Vereecken and R. Winand, *Revue ATB Mét.* **10** (1970) 147–50.

[19] *Idem, J. Electrochem. Soc.* **123** (1976) 643–46.

[20] *Idem, Surface Technology* **4** (1976) 227–35.

[21] G. Troch, 'Contribution à l'étude de l'influence d'inhibiteurs sur l'électrodéposition du cuivre en milieu sulfurique', Ph.D. Thesis, Université Libre de Bruxelles (1983).

[22] G. Troch, M. Degrez and R. Winand, *Electrochem. Soc.* **84-1** (May 1984) 406–7.

[23] M. Lambert and R. Winand, *Oberfläche/Surface* **18** (1977) 208–16.

[24] M. Degrez, 'Contribution à l'étude de l'électrodéposition du cuivre à haute densité de courant', Ph.D. Thesis, Université Libre de Bruxelles (1981).

[25] M. Degrez and R. Winand, *Electrochim. Acta* **29** (1984) 365-72.

[26] A. Weymeersch, R. Winand and L. Renard, *Plating and Surface Finishing* **68** (1981) 56–60.

[27] A. Weymeersch, R. Winand and L. Renard, *ibid.* **68** (1981) 118–20.

[28] G. Parissis, 'Contribution à l'étude de l'électrodéposition du manganèse à haute densité de courant', Ph.D. Thesis, Université Libre de Bruxelles (1982).

[29] G. Parissis and R. Winand, in 'Chloride electrometallurgy', (edited by P. D. Parker), Conf. Proc. TMS, 111th AIME annual meeting, Dallas (February 1982) pp. 131–54.

[30] A. Weymeersch, L. Renard, J. J. Conreur, R. Winand, M. Jorda and C. Pellet, *Plating and Surface Finishing* **73** (1986) 68–73.

[31] A. Rodriguez Fajardo, 'Contribution à l'étude de l'électrodéposition des alliages zinc–fer à haute densité de courant en solution sulfurique', Ph.D. Thesis, Université Libre de Bruxelles (1987).

[32] A. Rodriguez Fajardo, R. Winand, A. Weymeersch and L. Renard, Fundamental aspects of zinc–iron alloys electrodeposition, Fifth Continuous strip plating symposium American Electroplaters and Surface Finishers Society, Dearborn MI (May 1987).

[33] H. M. Wang, S. F. Chen, T. J. O'Keefe, M. Degrez and R. Winand, paper submitted to *J. Appl. Electrochem* **19** (1989) 174–182.

[34] M. Degrez, A. Rodriguez Fajardo and R. Winand, Oberfläche – Surface **30** (1989) (8) 20–28; (9) 14–20.

[35] R. Winand, High current density electroplating – 12th World Congress on surface finishing, Interfinish 88 Paris, (October 1988) *Proceedings*, Vol. 1, pp. 189–202.

[36] R. Winand, Surface and Coatings Technology **37** (1989) 65–87.

[37] R. Winand, 'Electrodeposition technology, theory and practice', Electrochem. Soc., Vol. **87-17** (1987) pp. 207–32.

[38] I. H. Warren (editor), 'Application of polarization measurements in the control of metal deposition', Elsevier, Amsterdam (1984).

[39] R. Weil and R. G. Barradas (editors), Proc. of a symp. on Electrocrystallization, Vol. **81-6**, Electrochem. Soc., Pennington (1981).

[40] L. T. Romankiw and D. R. Turner, Proc. of a symp. on Electrodeposition Technology, theory and practice, Vol. **87-17**, Electrochem. Soc., Pennington (1987).

[41] Extended abstracts of the Fall Meeting of the Electrochemical Society, San Diego CA, October 19–24 (1986), Vol. **86-2**, Section on electrodeposition.